

See discussions, stats, and author profiles for this publication at: <https://www.researchgate.net/publication/231644572>

# Bonding of Oxygen at the Oxide/Nanocrystal Interface of Oxidized Silicon Nanocrystals: An Ab Initio Study

ARTICLE *in* THE JOURNAL OF PHYSICAL CHEMISTRY C · APRIL 2010

Impact Factor: 4.77 · DOI: 10.1021/jp100632u

---

CITATIONS

29

READS

34

## 3 AUTHORS, INCLUDING:



Xiaodong Pi

Zhejiang University

81 PUBLICATIONS 881 CITATIONS

[SEE PROFILE](#)



Deren Yang

Zhejiang University

737 PUBLICATIONS 11,119 CITATIONS

[SEE PROFILE](#)

# Bonding of Oxygen at the Oxide/Nanocrystal Interface of Oxidized Silicon Nanocrystals: An *Ab Initio* Study

Xiaobo Chen, Xiaodong Pi, and Deren Yang\*

State Key Laboratory of Silicon Materials and Department of Materials Science and Engineering,  
Zhejiang University, Hangzhou, 310027, China

Received: January 22, 2010; Revised Manuscript Received: April 6, 2010

*Ab initio* methods based on density functional theory are employed to investigate the bonding of oxygen (O) at the oxide/nanocrystal (NC) interface after hydrogen (H)-passivated silicon (Si) NCs are oxidized. Besides the well-known quantum confinement effect, the type of O bonding and the oxidation state of Si at the oxide/NC interface are found to significantly affect the optical properties of oxidized Si NCs. After oxidation, the excitation energies of  $\text{Si}_{35}$  and  $\text{Si}_{66}$  increase, while those of  $\text{Si}_{87}$  and  $\text{Si}_{123}$  decrease. We show that oxidation-induced redshifts in the light emission from Si NCs do not always result from defective O such as doubly bonded O at the oxide/NC interface. When Si atoms at the oxide/NC interface are mainly in low oxidation states, backbond O at the interface *per se* results in the redshifts in the light emission from Si NCs. When Si atoms at the oxide/NC interface are mainly in high oxidation states,  $\text{Si}^{3+}=\text{O}$  at the interface leads to the redshifts in the light emission from Si NCs. It is found that for Si NCs with perfect oxide/NC interface (i.e., O at the interface is all backbond O) the seriously weakened next-nearest-neighboring Si–Si of  $\text{Si}^{3+}$  readily breaks after excitation. At the oxide/NC interface,  $\text{Si}^{2+}=\text{O}$  induced strong electronic localization and  $\text{Si}^{2+}=\text{O}$  and  $\text{Si}^{3+}=\text{O}$  induced reduction of interface polarization stabilize the geometry of oxidized Si NCs at the excited state. The electronic localization of severely stressed bridge O at the oxide/NC interface is relatively weak. This facilitates the breaking of nearest-neighboring Si–Si at the oxide/NC interface as oxidized Si NCs are excited.

## 1. Introduction

Silicon (Si) does not efficiently emit light because it is an indirect-bandgap semiconductor. It is of great interest to realize efficient light emission from Si to expand the application of Si from microelectronics to optoelectronics,<sup>1–7</sup> photovoltaics,<sup>8</sup> and bioimaging.<sup>9</sup> Among all kinds of methods to increase the efficiency of light emission from Si, the utilization of Si nanocrystals (NCs) has been very promising. It has been demonstrated that the basic mechanism for the light emission from Si NCs is the size-reduction-induced quantum confinement effect.<sup>10–14</sup> With a decrease in the Si NC size, the bandgap of Si NCs increases, leading to the blueshift of light emission from Si NCs. A decrease in the Si NC size also results in an increase in the probability of electron–hole recombination without the participation of phonons,<sup>15</sup> and thus an increase in light emission efficiency. In addition, it has been found that the light emission from Si NCs may be significantly affected by the surface states of Si NCs.<sup>16–19</sup> This is well exemplified by the effect of oxygen-related surface states on the light emission from Si NCs. Wolkin et al. found  $\sim 1$  eV redshifts in the light emission from Si NCs smaller than 3 nm after they were exposed to the atmosphere.<sup>20</sup> The redshifts were thought to be due to  $\text{Si}=\text{O}$  at the surface of Si NCs, as also indicated by Luppi's work.<sup>21</sup> However, Vasiliev et al. showed that bridge O connecting two Si atoms ( $\text{Si}–\text{O}–\text{Si}$ ) at the surface of Si NCs might also reduce the bandgap of Si NCs remarkably.<sup>22</sup> Luppi et al.'s calculation<sup>23</sup> demonstrated that the energy of luminescence related to  $\text{Si}–\text{O}–\text{Si}$  at the surface of Si NCs was 1.5 eV, consistent with that obtained in Ma et al.'s experiment.<sup>24</sup>

The O-related surface states were usually studied by using a simplified model, in which a single O atom was added onto the surface of a H-passivated Si NC. This simplification resulted in the bonding of O at the surface of Si NCs, which remained to be dominantly covered by H. In fact, O is usually introduced during oxidation. The surface of Si NCs after oxidation is actually the oxide/NC interface. Therefore, a model that incorporates the oxide/NC interface is more realistic in the study on O-related surface states. Once the formation of the oxide/NC interface is considered, the size reduction of Si NCs induced by oxidation is inherently involved. This facilitates a theoretical comparison in the light emission from Si NCs before and after oxidation in terms of both O-related surface states and size effect.

Zhou et al.<sup>25</sup> simulated the formation of the oxide/NC interface by passivating dangling bonds with OH groups at the surface of Si NCs. The size reduction of Si NCs associated with the formation of the oxide/NC interface was clearly absent. In Ramos et al.'s work,<sup>26,27</sup> an experimentally proved backbond-oxidation model<sup>20</sup> was adopted. They showed that  $\text{Si}=\text{O}$  and bridge O hardly affected the light emission from Si NCs. This was likely due to the fact that  $\text{Si}=\text{O}$  and bridge O were placed at the surface of oxidized Si NCs, rather than at the oxide/NC interface. It should be noted that the relaxed geometry of oxidized Si NCs at the excited state was often not considered in previous work. This led to an incomplete understanding on the underlying mechanisms for the light emission from oxidized Si NCs.

In this work, we use the backbond-oxidation model to form the oxide/NC interface. Calculations based on density functional theory (DFT) have been carried out to investigate the effect of

\* Corresponding author. E-mail: mseyang@zju.edu.cn.

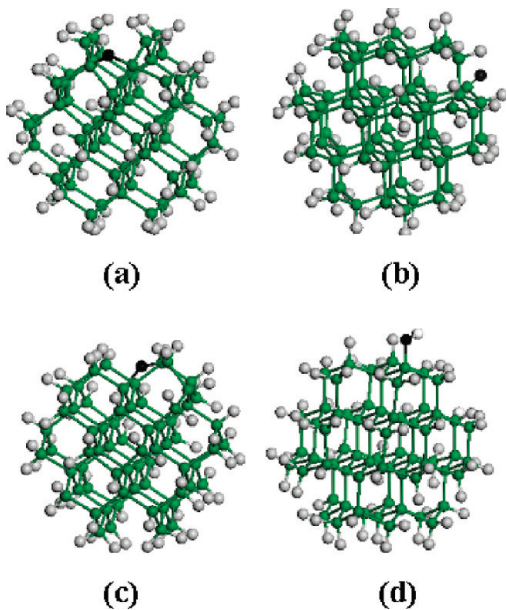


**Figure 1.** Optimized H-passivated NC models for Si<sub>66</sub> with (a) bridge O, (b) doubly bonded O, (c) backbond O, or (d) OH at the surface. O, Si, and H atoms are denoted by black, green, and gray spheres, respectively.

O bonding at the oxide/NC interface on the optical properties of oxidized Si NCs. Three configurations of O bonding at the oxide/NC interface (backbond O, Si=O, and bridge O) are considered. The relaxed geometry of oxidized Si NCs at the excited state is carefully examined. It is found that, besides the well-known quantum confinement effect, the type of O bonding and the oxidation state of Si at the oxide/NC interface significantly affect the optical properties of oxidized Si NCs.

## 2. Model and Method

The model of an original Si NC was constructed by cutting out a spherical portion in an optimized bulk Si model, in which the bond length of Si–Si was 2.36 Å. The NC surface was passivated by H atoms, consistent with most of the experimental observations. Si<sub>35</sub>H<sub>36</sub>, Si<sub>66</sub>H<sub>64</sub>, Si<sub>87</sub>H<sub>76</sub>, and Si<sub>123</sub>H<sub>74</sub> were studied in this work. They were 1.0, 1.4, 1.6, and 1.9 nm in diameter, respectively. A Si atom at the surface of these Si NCs was linked to one or two H atoms, as adopted in previous theoretical calculations.<sup>18,22,23</sup>

When the oxidation of H-passivated Si NCs started, the O incorporation likely led to the formation of bridge O, Si=O, backbond O, and OH at the surface, as illustrated in Figure 1. To evaluate the relative stability of these four configurations of O, we calculated their formation energies  $E_f$  by use of the following equation:<sup>28</sup>

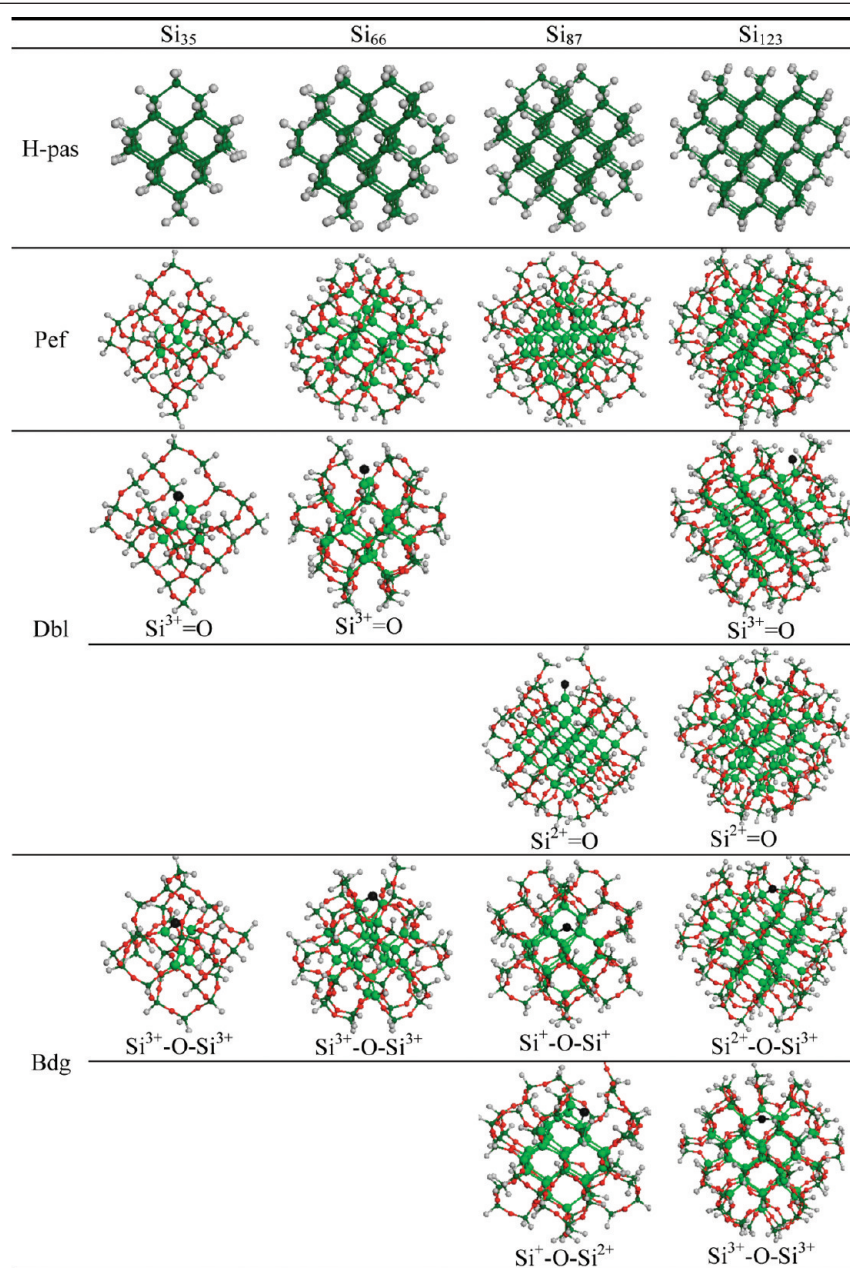
$$E_f(\text{Si}_m\text{H}_n\text{O}) = E_{\text{total}}(\text{Si}_m\text{H}_n\text{O}) - m\mu_{\text{Si}} - \frac{1}{2}n\mu_{\text{H}_2} - \frac{1}{2}\mu_{\text{O}_2}$$

$E_{\text{total}}$  was the total energy of an oxidized NC ( $\text{Si}_m\text{H}_n\text{O}$ ).  $\mu_{\text{Si}}$ ,  $\mu_{\text{H}_2}$ , and  $\mu_{\text{O}_2}$  were the chemical potentials of Si, H<sub>2</sub>, and O<sub>2</sub> at 0 K, respectively. The calculations showed that formation energies increased in the order of backbond O, OH, bridge O, and Si=O. For example, when the oxidized Si atom at the surface of Si<sub>66</sub>H<sub>64</sub> was originally passivated by two H atoms, the formation energies of backbond O, OH, bridge O, and Si=O were -6.82, -6.12, -5.86, and -4.79 eV, respectively. It was found that the formation energies varied as the original H passivation of

the oxidized Si atom was different. The aforementioned order of formation energies, however, did not change. In other words, the formation energy of backbond O was always the lowest. Therefore, the oxidation of Si NCs was simulated by inserting O at Si–Si backbonds in this work. Since the formation of OH did not follow that of backbond O within a certain period of time,<sup>20</sup> H passivation remained after the incorporation of backbond O. The oxidation resulted in shrunk Si-NC cores surrounded by single-layer oxide. Oxidized Si NCs with a perfect oxide/NC interface (i.e., O at the interface was all backbond O) were denoted by Pef. In spite of the highest formation energy for Si=O, the actual formation of Si=O had been demonstrated both theoretically<sup>29</sup> and experimentally.<sup>30</sup> Given that the formation energy of bridge O was lower than that of Si=O, bridge O could also be formed. Hence, it was possible that Si=O and bridge O appeared at the oxide/NC interface. We denoted the corresponding oxidized Si NCs as Dbl and Bdg, respectively. The relaxed geometries for Pef-, Dbl-, and Bdg-type oxidized Si NCs together with those for originally H-passivated Si NCs at the ground state have been shown in Table 1. It is noted that the bonding of doubly bonded O and bridge O may vary in terms of the oxidation state of Si to which O is bonded.

The optimization of Si NC structures and the calculation of total energies were performed with the modeling program DMOL3. *Ab initio* methods based on all-electron density functional theory (DFT) were used. In DFT, the Becke–Lee–Yang–Parr (BLYP) exchange-correlation functional<sup>31,32</sup> in the self-consistent field (SCF) iteration calculations was adopted. The double numerical basis sets augmented with p-polarization functions (DNP basis sets) were used in all of the calculations. While the size of the DNP basis sets was comparable to that of Gaussian 6-31G\*\* sets, the accuracy of DNP basis sets was much higher than that of Gaussian 6-31G\*\* sets. An orbital cutoff radius of 0.46 nm was used for the basis functions. A high SCF convergence threshold of 10<sup>-6</sup> was adopted. The maximum forces on all of the atoms in the optimized structures were less than 0.002 Ha/Å.

The calculation on the excited state followed a method used in previous papers.<sup>33,34</sup> When a Si NC was excited, an electron in the highest occupied molecular orbit (HOMO) transited to the lowest unoccupied molecular orbit (LUMO), leaving a hole in the HOMO. After the HOMO–LUMO transition, the relaxed geometry of the Si NC at the excited state was obtained by structural and electronic optimization. For both the ground state and excited state, the HOMO–LUMO gaps were readily calculated once the Si NC optimization was finished. For a Si NC larger than 1 nm, the excitation energy of the NC was similar to the HOMO–LUMO gap of the NC at the ground state.<sup>18,33</sup> The emission energy of the NC was similar to the HOMO–LUMO gap of the NC at the excited state. Therefore, we assumed that the HOMO–LUMO gaps at the ground state and excited state were approximately equal to the excitation energy and emission energy, respectively. This led to an error smaller than 0.06 eV. Given that the number of electrons in occupied states was odd after excitation, spin polarization should be introduced in the calculations on the excited state to obtain physically meaningful results. Large differences of 0.1–0.4 eV in the HOMO–LUMO gaps for the NCs at the excited state occurred if the spin polarization was not taken into account. We found that the excitation energies obtained by using DFT were close to those obtained by using time-dependent DFT (TDDFT). For example, for Si<sub>29</sub>H<sub>36</sub>, we obtained an excitation energy of 3.92 eV with BLYP-DFT, similar to that of 3.84 eV

TABLE 1: Relaxed Geometries for H-Passivated and Oxidized Si NCs with Different Sizes at the Ground State<sup>a</sup>

<sup>a</sup> O atoms in oxide are denoted by red spheres, while doubly bonded O atoms and bridge-O atoms at the oxide/NC interface are denoted by black spheres. Si atoms in oxide are denoted by dark green spheres, while those in the cores are denoted by green spheres. H atoms are denoted by grey spheres.

with BP-TDDFT.<sup>35</sup> However, our result was lower than the excitation energy of 4.52 eV obtained by using B3LYP-TDDFT.<sup>35</sup>

Oscillator strengths and radiative recombination rates for Si NCs with different sizes were numerically calculated in momentum space by using Fermi's golden rule.<sup>36</sup> The wave functions of the HOMO and LUMO at the ground state were used to obtain the momentum-matrix elements for the calculation of oscillator strengths. In the calculation of radiative recombination rates, the wave functions of the HOMO and LUMO at the excited state were employed. The matrices of the wave function used in the calculations were obtained by discretely sampling three-dimension space with a grid space of 0.2 Å. This grid space was tested to be sufficiently small for the accurate calculation of momentum-matrix elements.

### 3. Results and Discussion

**3.1. Si NCs at Ground State.** Figure 2a shows the HOMO–LUMO gaps of Si NCs with different sizes at the ground state before and after oxidation. It is seen that the HOMO–LUMO gap of H-passivated Si NCs increases with a decrease of NC size, consistent with the quantum confinement effect. When the perfect oxide/NC interface is formed, the HOMO–LUMO gaps of Si<sub>35</sub> and Si<sub>66</sub> increase, while those of Si<sub>87</sub> and Si<sub>123</sub> decrease. We calculate the average length of Si–Si bonds in the NC cores after oxidation, as shown in Figure 3. It is seen that for Si<sub>66</sub> the average length of Si–Si bonds is unchanged after oxidation. The increase in the HOMO–LUMO gap of Si<sub>66</sub> is due to the enhancement of the quantum confinement effect induced by oxidation. For Si<sub>35</sub>, oxidation

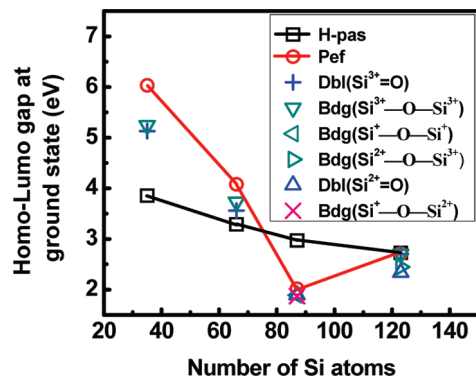


**Figure 2.** HOMO–LUMO gaps of Si NCs with different sizes at the ground state before and after oxidation. The surface of Si NCs is passivated by H before oxidation. A variety of configurations of O bonding at the oxide/NC interface are investigated for oxidized Si NCs.

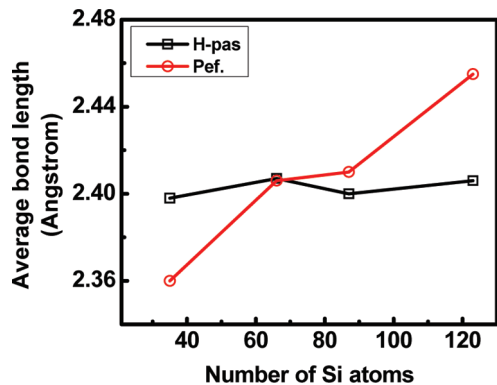
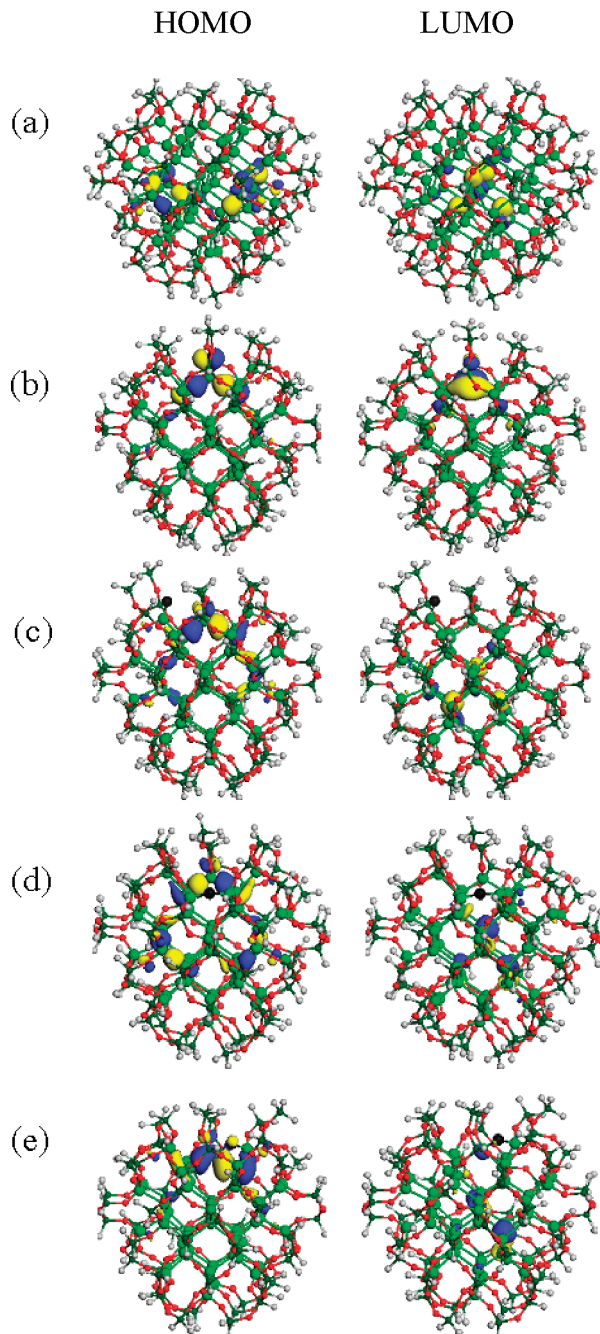


**Figure 3.** Average bond length of Si–Si bonds in the cores of Si NCs with different sizes at the ground state before and after oxidation. The surface of Si NCs is passivated by H before oxidation. The oxide/NC interface in the oxidized Si NCs is perfect (i.e., only with backbond O).

leads to a significant decrease in the average length of Si–Si bonds in the NC core (Figure 3). The compression of Si–Si bonds enlarges the separation between the  $\sigma$  bonding state and  $\sigma^*$  antibonding state.<sup>37</sup> In addition, the quantum confinement effect is also enhanced by oxidation. Hence, we see a significant increase (~56%) in the HOMO–LUMO gap. For  $\text{Si}_{87}$  and  $\text{Si}_{123}$  after oxidation, the average lengths of Si–Si bonds in the NC cores increase. Since the stretching of Si–Si bonds reduces the separation between the  $\sigma$  bonding state and  $\sigma^*$  antibonding state,<sup>37</sup> the enhancement of the quantum confinement effect induced by oxidation is negated. Therefore, the HOMO–LUMO gaps of  $\text{Si}_{87}$  and  $\text{Si}_{123}$  actually decrease. It is noted that the HOMO–LUMO gap of  $\text{Si}_{87}$  is significantly reduced after oxidation. This may not solely result from the stretching of Si–Si bonds.

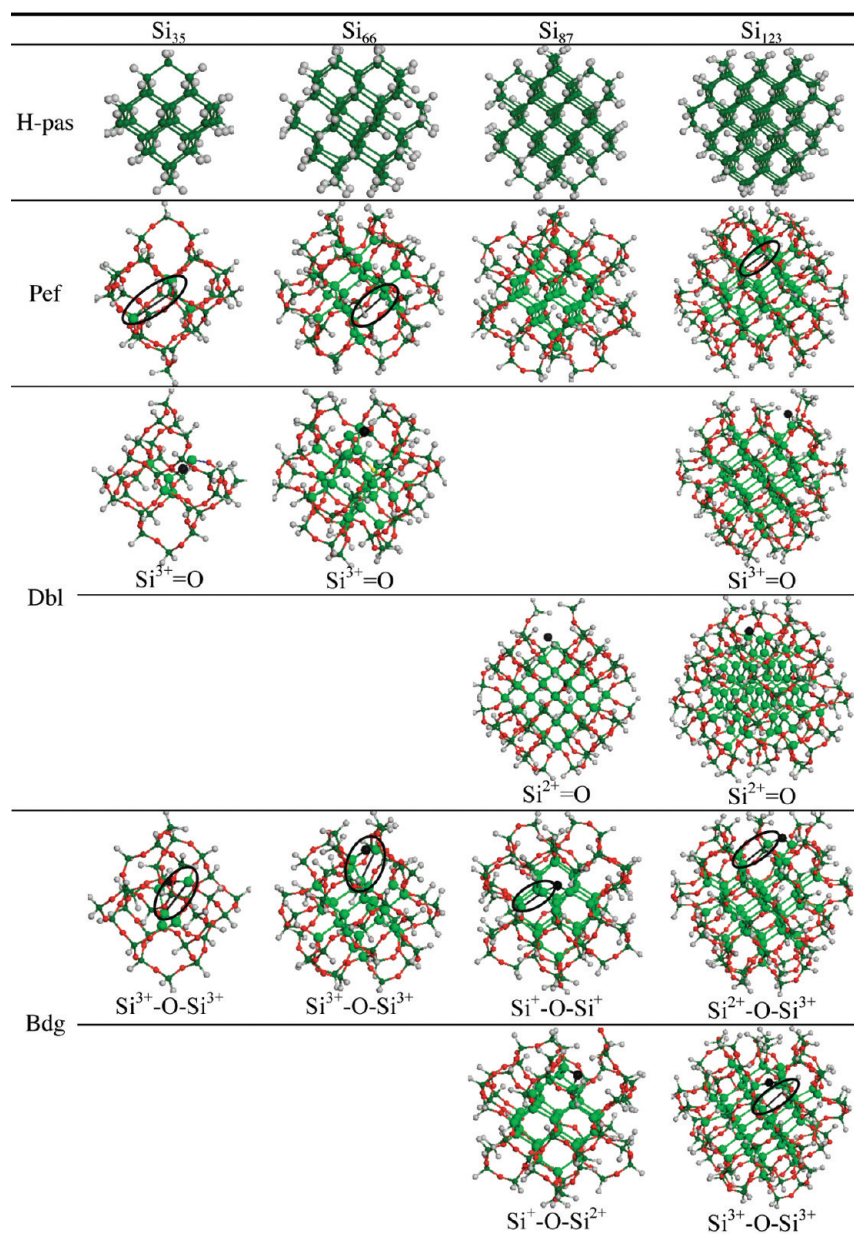
Si may be in three oxidation states ( $\text{Si}^+$ ,  $\text{Si}^{2+}$ ,  $\text{Si}^{3+}$ ) at the oxide/NC interface.<sup>38</sup> It has been shown that the localization of electronic states at oxidized Si decreases as the oxidation state changes from  $\text{Si}^+$  to  $\text{Si}^{2+}$  and then to  $\text{Si}^{3+}$ .<sup>39</sup> In this work, only  $\text{Si}^{3+}$  exists at the oxide/NC interface for  $\text{Si}_{35}$  and  $\text{Si}_{66}$ .  $\text{Si}^{2+}$  and  $\text{Si}^+$  (20 vs 80%) are at the oxide/NC interface for  $\text{Si}_{87}$ .  $\text{Si}^{2+}$  and  $\text{Si}^+$  (25 vs 75%) exist at the oxide/NC interface for  $\text{Si}_{123}$ . It is clear that most of the Si atoms at the oxide/NC interface for  $\text{Si}_{87}$  are in the lowest oxidation state, leading to the significant localization of electronic states. Hence, the HOMO–LUMO gap of  $\text{Si}_{87}$  is severely reduced after oxidation.

When doubly bonded O or bridge O is introduced at the oxide/NC interface, the HOMO–LUMO gap of an oxidized Si



**Figure 4.** Distribution of electron wave function for the HOMO and LUMO of oxidized  $\text{Si}_{123}$  with (a) a perfect oxide/NC interface or a (b)  $\text{Si}^{2+}=\text{O}$ , (c)  $\text{Si}^{3+}=\text{O}$ , (d)  $\text{Si}^{3+}-\text{O}-\text{Si}^{3+}$ , or (e)  $\text{Si}^{2+}-\text{O}-\text{Si}^{3+}$  bond at the oxide/NC interface at the ground state.

NC may be altered, as illustrated in Figure 2. Figure 4 shows the distribution of the electron wave function of oxidized  $\text{Si}_{123}$  with (a) a perfect oxide/NC interface and a (b)  $\text{Si}^{2+}=\text{O}$ , (c)  $\text{Si}^{3+}=\text{O}$ , (d)  $\text{Si}^{3+}-\text{O}-\text{Si}^{3+}$ , or (e)  $\text{Si}^{2+}-\text{O}-\text{Si}^{3+}$  bond at the oxide/NC interface. It is seen that the perfect oxide/NC interface is characterized by a delocalized electron wave function. Owing to a strong interaction between the  $\text{Si}^{2+}=\text{O}$  and the NC core, the electron wave functions of the HOMO and LUMO are significantly localized at the  $\text{Si}^{2+}=\text{O}$  bond (Figure 4b). Thus, the HOMO–LUMO gap is reduced compared to that of  $\text{Si}_{123}$  with the perfect oxide/NC interface (Figure 2). In contrast, if a  $\text{Si}^{3+}=\text{O}$  bond is at the oxide/NC interface for  $\text{Si}_{123}$ , the electronic localization at  $\text{Si}^{3+}=\text{O}$  is weak (Figure 4c). This is because the interaction between the  $\text{Si}^{3+}=\text{O}$  and the NC core is weak. A

TABLE 2: Relaxed Geometries for H-Passivated and Oxidized Si NCs with Different Sizes at the Excited State<sup>a</sup>

<sup>a</sup> O atoms in oxide are denoted by red spheres, while doubly bonded O atoms and bridge-O atoms at the oxide/NC interface are denoted by black spheres. Si atoms in oxide are denoted by dark green spheres, while those in the cores are denoted by green spheres. H atoms are denoted by grey spheres. Broken Si—Si bonds are indicated by black lines within ellipses.

similarly weak electronic localization is observed for  $\text{Si}^{3+}-\text{O}-\text{Si}^{3+}$  (Figure 4d). Therefore, the HOMO–LUMO gap after the incorporation of  $\text{Si}^{3+}=\text{O}$  or  $\text{Si}^{3+}-\text{O}-\text{Si}^{3+}$  is close to that of  $\text{Si}_{123}$  with the perfect oxide/NC interface (Figure 2). Figure 4e shows that the electronic localizations of the HOMO and LUMO for  $\text{Si}^{2+}-\text{O}-\text{Si}^{3+}$  are moderate, leading to a small decrease in the HOMO–LUMO gap (Figure 2).

When  $\text{Si}^{3+}=\text{O}$  or  $\text{Si}^{3+}-\text{O}-\text{Si}^{3+}$  is incorporated at the oxide/NC interface for  $\text{Si}_{35}$  and  $\text{Si}_{66}$ , the electronic localizations of the HOMO and LUMO are large enough (not shown) to decrease the HOMO–LUMO gaps (Figure 2). It is interesting that the HOMO–LUMO gap of oxidized  $\text{Si}_{87}$  hardly changes as a defective oxygen atom is introduced at the oxide/NC interface with a variety of configurations of bonding. This is due to the already existing significant electronic localization induced by  $\text{Si}^+$ .

**3.2. Si NCs at Excited State.** The optimized structures of H-passivated or oxidized  $\text{Si}_{35}$ ,  $\text{Si}_{66}$ ,  $\text{Si}_{87}$ , and  $\text{Si}_{123}$  at the first excited state are shown in Table 2. We have verified that the oscillator strengths of the first electronic transitions for all of the NCs in this work are in the range from  $10^{-6}$  to  $10^{-2}$ . This means that all of the first electronic transitions are dipole-allowed, although they may be weak. It is seen that for  $\text{Si}_{35}$ ,  $\text{Si}_{66}$ , and  $\text{Si}_{123}$  a Si—Si bond near the perfect oxide/NC interface breaks after excitation. In contrast, no Si—Si bonds break at the perfect oxide/NC interface after excitation for  $\text{Si}_{87}$ . For Si NCs with all four sizes, after excitation, a Si—Si bond breaks near the oxide/NC interface with bridge O (except for  $\text{Si}_{87}$  with  $\text{Si}^+-\text{O}-\text{Si}^{2+}$  at the oxide/NC interface), while there is no broken bond near the oxide/NC interface with doubly bonded O.

We know that a Si—O bond is essentially polarized. The valence electrons of the Si atom shift to the O atom because

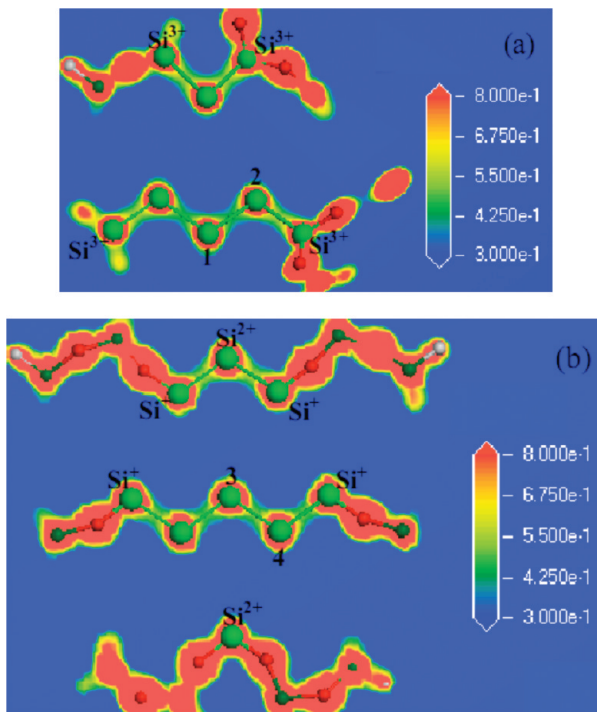


**Figure 5.** Distribution of electron density at the (110) plane for oxidized (a)  $\text{Si}_{66}$  and (b)  $\text{Si}_{87}$  with a perfect oxide/NC interface at the ground state. The (110) plane is obtained by cutting a NC through the diameter of the NC.

The O atom is very electronegative. This leads to the weakening of the next-nearest-neighboring (NNN)  $\text{Si}-\text{Si}$  bond. If the number of O atoms connected to a Si atom increases (i.e., the oxidation state of a Si atom increases), the weakening of the NNN  $\text{Si}-\text{Si}$  bond is aggravated. This is representatively demonstrated in Figure 5 that shows the distribution of electron density at the (110) plane for oxidized (a)  $\text{Si}_{66}$  and (b)  $\text{Si}_{87}$  with a perfect oxide/NC interface. It is seen that the electron density at the 1–2 Si–Si bond is lower than that at the 3–4 Si–Si bond. This is consistent with the fact that the oxidation state of the neighboring Si at the interface for the 1–2 Si–Si bond is higher than that of the neighboring Si at the interface for the 3–4 Si–Si bond ( $\text{Si}^{3+}$  vs  $\text{Si}^+$ ). For  $\text{Si}_{35}$ ,  $\text{Si}_{66}$ , and  $\text{Si}_{123}$  with a perfect oxide/NC interface, the seriously weakened NNN Si–Si bonds of  $\text{Si}^{3+}$  readily break after excitation (Table 2). For  $\text{Si}_{87}$ , the majority of Si atoms at the perfect oxide/NC interface are in the low oxidation state (+1). Therefore, the NNN Si–Si bonds are not weakened enough to be broken after excitation.

A  $\text{Si}=\text{O}$  bond typically consists of a  $\sigma$  bond and a  $\pi$  bond, leading to lower electronegativity compared with two  $\text{Si}-\text{O}$  bonds. Thus, the polarization at the interface is reduced after the incorporation of a  $\text{Si}=\text{O}$  bond (either  $\text{Si}^{2+}=\text{O}$  or  $\text{Si}^{3+}=\text{O}$ ), stabilizing the geometries of the excited state. As demonstrated before,  $\text{Si}^{2+}=\text{O}$  can strongly localize the frontier orbitals of the HOMO and LUMO (Figure 4b). This actually results in a screening for the NC core. In excitation, electron transition can only lead to small and local relaxation on the  $\text{Si}^{2+}=\text{O}$  bond, introducing a negligible effect on the NC core. The reduced interface polarization (induced by  $\text{Si}^{2+}=\text{O}$  and  $\text{Si}^{3+}=\text{O}$ ) and the strong electronic localization (only induced by  $\text{Si}^{2+}=\text{O}$ ) stabilize the geometry of oxidized Si NCs at the excited state (Table 2). The  $\text{Si}=\text{O}$  induced stabilization of NC geometry at the excited state has been previously observed in Li et al.'s work on Si NCs without the oxide/NC interface.<sup>40</sup>

As a bridge O atom is incorporated at the oxide/NC interface, the oxidation state of Si and thus the interface polarization do

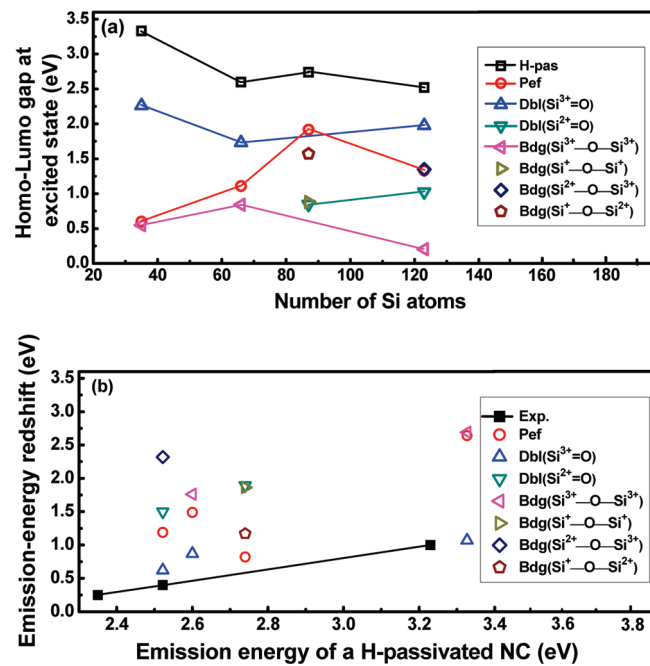


**Figure 6.** (a) HOMO–LUMO gaps of H-passivated and oxidized Si NCs with different sizes at the excited state. (b) Oxidation-induced redshifts in emission energy for Si NCs with different sizes. A variety of configurations of O bonding at the oxide/NC interface are considered. The experimental results from ref 20 are included for comparison.

not change. However, the localization of the HOMO and LUMO are weakened compared to the case for  $\text{Si}^{2+}=\text{O}$  (Figure 4). Therefore, the screening effect induced by bridge O is not as significant as that induced by  $\text{Si}^{2+}=\text{O}$ . We notice that the incorporation of bridge O gives rise to a large structural shrinkage that seriously stretches the nearest-neighboring  $\text{Si}-\text{Si}$  bond. This stretching together with the reduced electronic screening causes the nearest-neighboring  $\text{Si}-\text{Si}$  bond to break after excitation. For  $\text{Si}_{87}$ , the incorporation of a  $\text{Si}^+-\text{O}-\text{Si}^{2+}$  bond at the oxide/NC interface only results in a change of bond angle for the nearest-neighboring  $\text{Si}-\text{Si}-\text{Si}$ . The absence of bond stretching leads to no bond breaking after excitation.

We have obtained the HOMO–LUMO gaps for H-passivated or oxidized Si NCs at the excited state, as shown in Figure 6a. Since the HOMO–LUMO gap at the excited state approximates the emission energy, we can see that the emission energy of H-passivated Si NCs decreases with an increase in the NC size, consistent with the quantum confinement effect. According to Delerue et al.'s work,<sup>36</sup> the electron–hole recombination at dangling bonds induced by the breaking of  $\text{Si}-\text{Si}$  bonds near the oxide/NC interface is radiative in our work on Si NCs smaller than 2 nm. It is clear that after oxidation the emission energies of Si NCs with different sizes all decrease. The emission originating from oxidation-induced dangling bonds is actually in the infrared region. Although there is no breaking of  $\text{Si}-\text{Si}$  bonds in the case of  $\text{Si}=\text{O}$  incorporation, the strong electronic localization of  $\text{Si}=\text{O}$  causes the emission energies to remarkably decrease. Similar to what was discussed on the HOMO–LUMO gaps of oxidized Si NCs at the ground state, the oxidation states of Si at the oxide/NC interface affect the oxidation-induced redshifts (Figure 6a).

For all of the sizes of Si NCs with different types of oxide/NC interfaces, the oxidation-induced redshifts in light emission are compiled in Figure 6b. The experimental results from Wolkin et al.'s work<sup>20</sup> are also included for comparison. It is

**TABLE 3: Oscillator Strengths (OS) and Recombination Rates (R) for H-Passivated and Oxidized Si NCs<sup>a</sup>**

	Si <sub>35</sub>		Si <sub>66</sub>		Si <sub>87</sub>		Si <sub>123</sub>	
	OS	R (s <sup>-1</sup> )						
H-pas	1.8 × 10 <sup>-2</sup>	7.8 × 10 <sup>5</sup>	1.4 × 10 <sup>-2</sup>	6.4 × 10 <sup>8</sup>	3.1 × 10 <sup>-5</sup>	1.1 × 10 <sup>5</sup>	4.2 × 10 <sup>-3</sup>	8.8 × 10 <sup>2</sup>
oxidized	1.8 × 10 <sup>-3</sup>	5.5 × 10 <sup>8</sup>	7.7 × 10 <sup>-3</sup>	2.7 × 10 <sup>7</sup>	2.3 × 10 <sup>-5</sup>	5.9 × 10 <sup>5</sup>	2.5 × 10 <sup>-3</sup>	5.7 × 10 <sup>8</sup>

<sup>a</sup> The differences in emission energy between H-passivated and oxidized Si NCs are close to those obtained in ref 20.

found that Si<sup>3+</sup>=O is most likely responsible for the experimentally observed oxidation-induced redshifts in the light emission from Si<sub>35</sub>, Si<sub>66</sub>, and Si<sub>123</sub>, for which Si is mainly in the high oxidation state of +3 at the oxide/NC interface. It is interesting to note that for Si<sub>87</sub> the backbond O *per se* may lead to the oxidation-induced redshift. We find that Si at the oxide/NC interface is mainly in the low oxidation state of +1 if facets are formed at the oxide/NC interface after oxidation. This is the case for Si<sub>87</sub> (Table 1), which may very well apply to Si NCs with other sizes.<sup>38</sup> Therefore, the oxidation-induced redshifts in the light emission from Si NCs do not always result from doubly bonded O at the oxide/NC interface. The oxidation state of Si at the oxide/NC interface may determine which type of O at the interface significantly influences the light emission from oxidized Si NCs.

For all of the sizes, we have calculated both the oscillator strengths and recombination rates for oxidized Si NCs that emit light with energies closest to experimental values. The results together with those for H-passivated Si NCs are tabulated in Table 3. Generally speaking, the oscillator strength of a dipole-allowed transition is typically larger than 10<sup>-2</sup>, while that of a forbidden transition is smaller than 10<sup>-8</sup>. The oscillator strengths for both H-passivated and oxidized Si NCs fall in the range from 10<sup>-8</sup> to 10<sup>-2</sup>. Although the recombination rates increase (excluding Si<sub>66</sub>), the oscillator strengths decrease after oxidation. The decrease of an oscillator strength means that the probability of promoting a Si NC to its excited state decreases. Furthermore, there may be defects (e.g., dangling bonds) at the oxide/NC interface after oxidation.<sup>16</sup> Si–Si bonds near the oxide/NC interface may be broken after excitation. All of these probably contribute to the decrease in the efficiency of visible spectrum light emission from Si NCs after oxidation.<sup>16</sup>

#### 4. Conclusion

Within the framework of density functional theory, the effect of O bonding at the oxide/NC interface on the optical properties of Si NCs has been investigated. The oxide/NC interface has been simulated by an experimentally proved backbond-oxidation model. We show that after oxidation the excitation energy of a Si NC is not guaranteed to blueshift, while the emission energy of the Si NC definitely redshifts. When Si atoms at the oxide/NC interface are mainly in high oxidation states, Si<sup>3+</sup>=O at the interface leads to redshifts in the light emission from Si NCs. When Si atoms at the oxide/NC interface are mainly in low oxidation states, the backbond O at the interface *per se* results in the redshifts in the light emission from Si NCs. The strong electronic localization (induced by Si<sup>2+</sup>=O) and the reduced interface polarization (induced by Si<sup>2+</sup>=O and Si<sup>3+</sup>=O) stabilize the geometry of oxidized Si NCs at the excited state. When bridge O exists at the oxide/NC interface, weak electron localization and large structural stress facilitate the breaking of the nearest-neighboring Si–Si bond of bridge O during the excitation of oxidized Si NCs. In most cases for a Si NC with the perfect oxide/NC interface, the seriously weakened

NNN Si–Si bond of Si<sup>3+</sup> readily breaks after excitation. The light emission related to the dangling bonds induced by the breaking of Si–Si bonds is in the infrared region.

**Acknowledgment.** The authors are grateful to S. X. Li for helpful discussion. Shanghai Supercomputer Center is thanked for providing computation resources. This work was mainly supported by the National Basic Research Program of China (973 Program) under Grant No. 2007CB613403. Partial support from National Natural Science Foundation of China (Grant Nos. 50902122 and 50832006) and Research Fund for Doctoral Program of Higher Education of China (Grant No. 20090101120157) is acknowledged.

#### References and Notes

- (1) Canham, L. T. *Appl. Phys. Lett.* **1990**, 57, 1046.
- (2) Hirschman, K. D.; Tsybeskov, L.; Duttagupta, S. P.; Fauchet, P. M. *Nature* **1996**, 384, 338.
- (3) Pavesi, L.; Negro, L. D.; Mazzoleni, C.; Franzo, G.; Priolo, F. *Nature* **2000**, 408, 440.
- (4) Wang, M. H.; Li, D. S.; Yuan, Z.; Yang, D. R.; Que, D. L. *Appl. Phys. Lett.* **2007**, 90, 131903.
- (5) Heng, C. L.; Sun, Y. K.; Wang, S. T.; Chen, Y.; Qiao, Y. P.; Zhang, B. R.; Ma, Z. C.; Zong, W. H.; Qin, G. G. *Appl. Phys. Lett.* **2000**, 77, 1416.
- (6) Huang, R.; Dong, H.; Wang, D.; Chen, K.; Ding, H.; Wang, X.; Li, W.; Xu, J.; Ma, Z. *Appl. Phys. Lett.* **2008**, 92, 181106.
- (7) Milgram, J. N.; Wojcik, J.; Mascher, P.; knights, A. P. *Opt. Express* **2007**, 15, 14679.
- (8) Kim, S.-K.; Cho, C.-H.; Kim, B.-H.; Park, S.-J.; Lee, J. W. *Appl. Phys. Lett.* **2009**, 95, 143120.
- (9) He, Y.; Kang, Z.-H.; Li, Q.-S.; Tsang, C. H. A.; Fan, C.-H.; Lee, S.-T. *Angew. Chem., Int. Ed.* **2008**, 48, 128.
- (10) Pi, X. D.; Liptak, R. W.; Campbell, S. A.; Kortshagen, U. *Appl. Phys. Lett.* **2007**, 91, 083112.
- (11) Gupta, A.; Swihart, M. T.; Wiggers, H. *Adv. Funct. Mater.* **2009**, 19, 1.
- (12) Pi, X. D.; Liptak, R. W.; Nowak, J. D.; Wells, N. P.; Carter, C. B.; Campbell, S. A.; Kortshagen, U. *Nanotechnology* **2008**, 19, 245603.
- (13) Wang, L. W.; Zunger, A. *J. Phys. Chem.* **1994**, 98, 2158.
- (14) Ledoux, G.; Guillois, O.; Porterat, D.; Reynaud, C.; Huisken, F.; Kohn, B.; Paillard, V. *Phys. Rev. B* **2000**, 62, 15942.
- (15) Kovalev, D.; Heckler, H.; Ben-Chorin, M.; Polisski, G.; Schwartzkopff, M.; Koch, F. *Phys. Rev. Lett.* **1998**, 81, 2803.
- (16) Pi, X. D.; Mangolini, L.; Campbell, S. A.; Kortshagen, U. *Phys. Rev. B* **2007**, 75, 085423.
- (17) Qin, G. G.; Li, Y. *J. Phys. Rev. B* **2003**, 68, 085309.
- (18) Puzder, A.; Williamson, A. J.; Grossman, J. C.; Galli, G. *Phys. Rev. Lett.* **2002**, 88, 097401.
- (19) Reboredo, F. A.; Galli, G. *J. Phys. Chem. B* **2005**, 109, 1072.
- (20) Wolkin, M. V.; Jorne, J.; Fauchet, P. M.; Allan, G.; Delerue, C. *Phys. Rev. Lett.* **1999**, 82, 197.
- (21) Luppi, M.; Ossicini, S. *Phys. Status Solidi A* **2003**, 197 (1), 251.
- (22) Vasiliev, I.; Chelikowsky, J. R.; Martin, R. M. *Phys. Rev. B* **2002**, 65, 121302(R).
- (23) Luppi, E.; Iori, F.; Magri, R.; Pulci, O.; Ossicini, S.; Degoli, E.; Olevano, V. *Phys. Rev. B* **2007**, 75, 033303.
- (24) Ma, Z.; Liao, X.; Kong, G.; Chu, J. *Appl. Phys. Lett.* **1999**, 75, 1857.
- (25) Zhou, Z.; Brus, L.; Friesner, R. *Nano Lett.* **2003**, 3, 163.
- (26) Ramos, L. E.; Furthmüller, J.; Bechstedt, F. *Phys. Rev. B* **2004**, 70, 033311.
- (27) Ramos, L. E.; Furthmüller, J.; Bechstedt, F. *Phys. Rev. B* **2005**, 71, 035328.
- (28) Degoli, E.; Ossicini, S.; Cantele, G.; Luppi, E.; Magri, R.; Ninno, D.; Bisi, O. *Phys. Status Solidi C* **2005**, 2 (9), 3354.
- (29) Zhou, F.; Head, J. D. *J. Phys. Chem. B* **2000**, 104, 9981.

- (30) Chabal, Y. J.; Raghavachari, K.; Zhang, X.; Garfunkel, E. *Phys. Rev. B* **2002**, *66*, 161315(R).
- (31) Becke, A. D. *Phys. Rev. A* **1988**, *38*, 3098.
- (32) Lee, C.; Yang, W.; Parr, R. G. *Phys. Rev. B* **1988**, *37*, 785.
- (33) Degoli, E.; Cantele, G.; Luppi, E.; Magri, R.; Ninno, D.; Bisi, O.; Ossicini, S. *Phys. Rev. B* **2004**, *69*, 155411.
- (34) Ramos, L. E.; Weissker, H.-Ch.; Furthmüller, J.; Bechstedt, F. *Phys. Status Solidi B* **2005**, *242*, 3053.
- (35) Lehtonen, O.; Sundholm, D. *Phys. Rev. B* **2005**, *72*, 085424.
- (36) Delerue, C.; Allan, G.; lannoo, M. *Phys. Rev. B* **1993**, *48*, 11024.
- (37) Allan, G.; Delerue, C.; Lannoo, M. *Phys. Rev. Lett.* **1996**, *76*, 2961.
- (38) Thøgersen, A.; Diplas, S.; Mayandi, J.; Finstad, T.; Olsen, A.; Watts, J. F.; Mitome, M.; Bando, Y. *J. Appl. Phys.* **2008**, *103*, 024308.
- (39) Carrier, P. *Phys. Rev. B* **2009**, *80*, 075319.
- (40) Li, Q. S.; Zhang, R. Q.; Lee, S. T.; Niehaus, T. A.; Frauenheim, Th. *Appl. Phys. Lett.* **2007**, *91*, 043106.

JP100632U